ation by reconstitution with bone marrow or fetal liver cells from green fluorescent protein-gene transgenic mice, J. Cell Sci. 115 (2002) 1285–1293.

[6] M.A. LaBarge, H.M. Blau, Biological progression from adult bone marrow to mononucleate muscle stem cell to multinucleate muscle fiber in response to injury, Cell 111 (2002) 589–601.

[7] F.D. Camargo, R. Green, Y. Capetanaki, K.A. Jackson, M.A. Goodell, Single hematopoietic stem cells generate skeletal muscle through myeloid intermediates, Nat. Med. 9 (2003) 1520–1527.

[8] S.L. McKinney-Freeman, S.M. Majka, K.A. Jackson, K. Norwood, K.K. Hirschi, M.A. Goodell, Altered phenotype and reduced function of muscle-derived hematopoietic stem cells, Exp. Hematol. 31 (2003) 806–814.

[9] A. Asakura, P. Seale, A. Girgis-Gabardo, M.A. Rudnicki, Myogenic specification of side population cells in skeletal muscle, J. Cell Biol. 159 (2002) 123–134.

[10] S.M. Majka, K.A. Jackson, K.A. Kienstra, M.W. Majesky, M.A. Goodell, K.K. Hirschi, Distinct progenitor populations in skeletal muscle are bone marrow derived and exhibit different cell fates during vascular regeneration, J. Clin. Invest. 111 (2003) 71–79.

[11] E. Bachrach, S. Li, A.L. Perez, J. Schienda, K. Liadaki, J. Volinski, A. Flint, J. Chamberlain, L.M. Kunkel, Systemic delivery of human microdystrophin to regenerating mouse dystrophic muscle by muscle progenitor cells, Proc. Natl. Acad. Sci. USA 101 (2004) 3581–3586.

[12] S. Fukada, S. Higuchi, M. Segawa, K. Koda, Y. Yamamoto, K. Tsujikawa, Y. Kohama, A. Uezumi, M. Imamura, Y. Miyagoe-Suzuki, S. Takeda, H. Yamamoto, Purification and cell-surface marker characterization of quiescent satellite cells from murine skeletal muscle by a novel monoclonal antibody, Exp. Cell Res. 296 (2004) 245–255.

[13] P. Seale, L.A. Sabourin, A. Girgis-Gabardo, A. Mansouri, P. Gruss, M.A. Rudnicki, Pax7 is required for the specification of myogenic satellite cells, Cell 102 (2000) 777–786.

[14] K. Ojima, A. Uezumi, H. Miyoshi, S. Masuda, Y. Morita, A. Fukase, A. Hattori, H. Nakauchi, Y. Miyagoe-Suzuki, S. Takeda, Mac-1^{low} early myeloid cells in the bone marrow-derived SP fraction migrate into injured skeletal muscle and participate in muscle regeneration, Biochem. Biophys. Res. Commun. 321 (2004) 1050–1061.

[15] J.D. Allen, R.F. Brinkhuis, J. Wijnholds, A.H. Schinkel, The mouse Bcrp1/Mxr/Abcp gene: amplification and overexpression in cell lines selected for resistance to topotecan, mitoxantrone, or doxorubicin, Cancer Res. 59 (1999) 4237–4241.

[16] T.A. Rando, H.M. Blau, Primary mouse myoblast purification, characterization, and transplantation for cell-mediated gene therapy, J. Cell Biol. 125 (1994) 1275–1287.

[17] Z. Qu, L. Balkir, J.C. van Deutekom, P.D. Robbins, R. Pruchnic, J. Huard, Development of approaches to improve cell survival in myoblast transfer therapy, J. Cell Biol. 142 (1998) 1257–1267.

[18] R. Kasturi, V.C. Joshi, Hormonal regulation of stearoyl coenzyme A desaturase activity and lipogenesis during adipose conversion of 3T3-L1 cells, J. Biol. Chem. 257 (1982) 12224–12230.

[19] S. Zhou, J.D. Schuetz, K.D. Bunting, A.M. Colapietro, J. Sampath, J.J. Morris, I. Lagutina, G.C. Grosveld, M. Osawa, H. Nakauchi, B.P. Sorrentino, The ABC transporter Bcrp1/ABCG2 is expressed in a wide variety of stem cells and is a molecular determinant of the side-population phenotype, Nat. Med. 7 (2001) 1028–1034.

[20] M. Maliepaard, G.L. Scheffer, I.F. Faneyte, M.A. van Gastelen, A.C. Pijnenborg, A.H. Schinkel, M.J. van De Vijver, R.J. Scheper, J.H. Schellens, Subcellular localization and distribution of the breast cancer resistance protein transporter in normal human tissues, Cancer Res. 61 (2001) 3458–3464.

[21] J.W. Jonker, M. Buitelaar, E. Wagenaar, M.A. Van Der Valk, G.L. Scheffer, R.J. Scheper, T. Plosch, F. Kuipers, R.P. Elferink, H. Rosing, J.H. Beijnen, A.H. Schinkel, The breast cancer resistance protein protects against a major chlorophyll-derived dietary photo-

toxin and protoporphyria, Proc. Natl. Acad. Sci. USA 99 (2002) 15649–15654.

[22] F. Rivier, O. Alkan, A.F. Flint, K. Muskiewicz, P.D. Allen, P. Leboulch, E. Gussoni, Role of bone marrow cell trafficking in replenishing skeletal muscle SP and MP cell populations, J. Cell Sci. 117 (2004) 1979–1988.

[23] A.P. Meeson, T.J. Hawke, S. Graham, N. Jiang, J. Elterman, K. Hutcheson, J.M. Dimaio, T.D. Gallardo, D.J. Garry, Cellular and molecular regulation of skeletal muscle side population cells, Stem Cells 22 (2004) 1305–1320.

[24] S. Davis, T.H. Aldrich, P.F. Jones, A. Acheson, D.L. Compton, V. Jain, T.E. Ryan, J. Bruno, C. Radziejewski, P.C. Maisonpierre, G.D. Yancopoulos, Isolation of angiopoietin-1, a ligand for the TIE2 receptor, by secretion-trap expression cloning, Cell 87 (1996) 1161–1169.

[25] N. Takakura, T. Watanabe, S. Suenobu, Y. Yamada, T. Noda, Y. Ito, M. Satake, T. Suda, A role for hematopoietic stem cells in promoting angiogenesis, Cell 102 (2000) 199–209.

[26] M.J. Doherty, B.A. Ashton, S. Walsh, J.N. Beresford, M.E. Grant, A.E. Canfield, Vascular pericytes express osteogenic potential in vitro and in vivo, J. Bone Miner. Res. 13 (1998) 828–838.

[27] M.M. Levy, C.J. Joyner, A.S. Virdi, A. Reed, J.T. Triffitt, A.H. Simpson, J. Kenwright, H. Stein, M.J. Francis, Osteoprogenitor cells of mature human skeletal muscle tissue: an in vitro study, Bone 29 (2001) 317–322.

[28] S. Shi, S. Gronthos, Perivascular niche of postnatal mesenchymal stem cells in human bone marrow and dental pulp, J. Bone Miner. Res. 18 (2003) 696–704.

[29] M. Iurlaro, M. Scatena, W.H. Zhu, E. Fogel, S.L. Wieting, R.F. Nicosia, Rat aorta-derived mural precursor cells express the Tie2 receptor and respond directly to stimulation by angiopoietins, J. Cell Sci. 116 (2003) 3635–3643.

[30] R. Pola, L.E. Ling, M. Silver, M.J. Corbley, M. Kearney, R. Blake Pepinsky, R. Shapiro, F.R. Taylor, D.P. Baker, T. Asahara, J.M. Isner, The morphogen Sonic hedgehog is an indirect angiogenic agent upregulating two families of angiogenic growth factors, Nat. Med. 7 (2001) 706–711.

[31] R. Pola, L.E. Ling, T.R. Aprahamian, E. Barban, M. Bosch-Marce, C. Curry, M. Corbley, M. Kearney, J.M. Isner, D.W. Losordo, Postnatal recapitulation of embryonic hedgehog pathway in response to skeletal muscle ischemia, Circulation 108 (2003) 479–485.

[32] Y. Li, W. Foster, B.M. Deasy, Y. Chan, V. Prisk, Y. Tang, J. Cummins, J. Huard, Transforming growth factor-beta1 induces the differentiation of myogenic cells into fibrotic cells in injured skeletal muscle: a key event in muscle fibrogenesis, Am. J. Pathol. 164 (2004) 1007–1019.

[33] A.C. McPherron, A.M. Lawler, S.J. Lee, Regulation of skeletal muscle mass in mice by a new TGF-beta superfamily member, Nature 387 (1997) 83–90.

[34] S. Iezzi, M. Di Padova, C. Serra, G. Caretti, C. Simone, E. Maklan, G. Minetti, P. Zhao, E.P. Hoffman, P.L. Puri, V. Sartorelli, Deacetylase inhibitors increase muscle cell size by promoting myoblast recruitment and fusion through induction of follistatin, Dev. Cell 6 (2004) 673–684.

[35] A.G. Engel, E. Ozawa, Dystrophinopathies, in: A.G. Engel, C. Franzini-Armstrong (Eds.), Myology, McGraw-Hill, New York, 2004, pp. 961–1025.

[36] B.Q. Banker, A.G. Engel, Basic reactions of muscle, in: A.G. Engel, C. Franzini-Armstrong (Eds.), Myology, McGraw-Hill, New York, 2004, pp. 691–747.

[37] C. Farrington-Rock, N.J. Crofts, M.J. Doherty, B.A. Ashton, C. Griffin-Jones, A.E. Canfield, Chondrogenic and adipogenic potential of microvascular pericytes, Circulation 110 (2004) 2226–2232.

ORIGINAL ARTICLES

Intracellular Localization of Dysferlin and its Association with the Dihydropyridine Receptor

BERYL N. AMPONG[1,2], MICHIHIRO IMAMURA[1], TERUHIRO MATSUMIYA[2],
MIKIHARU YOSHIDA[1] AND SHIN'ICHI TAKEDA[1]

[1]Department of Molecular Therapy, National Institute of Neuroscience, National Center for Neurology
· and Psychiatry, 4-1-1 Ogawahigashi-cho, Kodaira, Tokyo 187-8502, Japan
[2]Department of Pharmacology, Tokyo Medical University, 6-1-1 Shinjuku, Tokyo 160-8402, Japan

Mutations in the dysferlin gene underlie two phenotypically distinct muscular dystrophies: Miyoshi myopathy and limb-girdle muscular dystrophy 2B. Dysferlin was proposed to have a putative functional role in mediating the fusion of intracellular vesicles to the sarcolemma during injury-induced membrane repair, but dysferlin has been found not only at the sarcolemma but also within the cytoplasm of skeletal muscle fibers by immunohistochemistry. In this study, we examined the subcellular localization of dysferlin in skeletal muscle by immunohistochemical and biochemical analyses to elucidate other functional roles of dysferlin. Immunohistochemistry confirmed granular cytoplasmic expression pattern of dysferlin in muscle fibers. Subcellular membrane fractionation revealed that a portion of dysferlin associated with a T-tubule-enriched intracellular membrane fraction as well as a sarcolemmal fraction. This indication was consistent with subsequent results that dysferlin coprecipitates by immunoprecipitation with the dihydropyridine receptor (DHPR), a protein complex localized in T-tubules. Moreover, both proteins were observed to partially colocalize by double immunofluorescent labeling in skeletal muscle fibers. We also found that caveolin-3, previously shown to interact with dysferlin, coprecipitates with DHPR. These results demonstrated that dysferlin may be involved in the formation of an oligomeric complex with DHPR and caveolin-3. Caveolin-3 has been also reported to participate in an insulin-regulated transport mechanism in muscle, and caveolin-3-containing vesicles might traffic between intracellular sites and target sites on the sarcolemma and T-tubules. Therefore, it is very intriguing to assume that dysferlin might be involved in the fusion of caveolin-3-containing vesicles with T-tubules.

Key Words: dysferlin, T-tubules, caveolin-3

Introduction

Two phenotypically distinct forms of muscular dystrophy with autosomal recessive inheritance, Miyoshi myopathy and limb girdle muscular dystrophy 2B (LGMD 2B) are reported to be caused by genetic mutations in the dysferlin gene (DYSF). Distal or proximal muscles are known to be predominantly involved in Miyoshi myopathy or in LGMD 2B, respectively [1,2]. Both diseases are clinically characterized by a late onset and slow progression of symptoms, as well as elevated serum creatine kinase levels [3]. DYSF was identified through positional cloning and mapped to the 2p13 gene locus [4,5]. It consists of over 55 exons transcribed into an 8.5 kb major transcript predominantly expressed in skeletal muscle [4,5].

The functional role of dysferlin in muscle physiology and pathology has been the subject of extensive research over the years. Studies of its cDNA sequence predict a protein of approximately 230 kDa, typically a type II transmembrane protein. Dysferlin contains sequences of calcium-binding C2 domains. These are motifs found in a number of proteins involved in signal transduction and membrane trafficking [6] such as the calcium-sensing synaptotagmins [7] and protein kinase C [8]. In addition, dysferlin has recently been identified as a member of a unique family of proteins: the ferlins. These proteins, which include myoferlin [9] and otoferlin [10], have as an important functional characteristic a high sequence homology to the C. elegans fer-1 protein, reported to play a critical role in the fusion of intracellular vesicles with the plasma membrane in sperm cells [11]. This has suggested a putative role for dysferlin in mediating the fusion of intracellular vesicles with the sarcolemma of skeletal muscle fibers in a calcium-dependent manner. Indeed, dysferlin knockout mice developed a slowly progressive muscular dystrophy due to an inability of intracellular vesicles

134

to fuse with the sarcolemma during injury-induced membrane repair [12]. The fusion process has also been suggested to involve an interaction between dysferlin and the annexins; calcium and phospholipid-binding proteins implicated in membrane repair [13]. The presence of dysferlin has been shown not only at the sarcolemma [12-16] but also within the cytoplasm [12,16] of skeletal muscle fibers by immunohistochemistry and it has been proposed that dysferlin present on the intracellular vesicles is involved in the injury-induced fusion process [17].

In the present study, we systematically examined the localization of dysferlin in the muscle fiber by immunohistochemical and biochemical analyses in order to characterize the intracellular localization of dysferlin. Our immunohistochemical results confirmed the presence of dysferlin at the sarcolemma and within the cytoplasm of muscle fibers. In membrane fractionation experiments, dysferlin was shown to be associated with a T-tubule-enriched intracellular membrane fraction in addition to a sarcolemmal fraction. This association with a T-tubule-enriched membrane fraction was consistent with subsequent results shown by immunoprecipitation experiments that dysferlin coprecipitates with the dihydropyridine receptor (DHPR), a protein complex localized in T-tubules. We also found that caveolin-3, previously shown to interact with dysferlin, coprecipitates with DHPR by immunoprecipitation.

Materials and methods

Animals

Wistar rats and mice (Balb/c and SJL) were purchased from Clea Japan Inc. (Tokyo, Japan) and Charles River Japan Inc. (Tokyo, Japan) respectively. The SJL mouse is a naturally occurring animal model of dysferlin deficiency caused by an inframe deletion mutation in the *dysferlin* gene. It has been shown that expression of truncated dysferlin is greatly reduced [18,19] in skeletal muscles of this animal model. All animal handling procedures were performed in accordance with protocols approved by the National Institute of Neuroscience, NCNP, Kodaira, Japan.

Antibodies

For immunoprecipitation studies, a polyclonal antibody against dysferlin was raised by immunizing rabbits with a polypeptide corresponding to the amino acid sequence of human dysferlin 1999 to 2016 conjugated with keyhole limpet hemocyanin, and emulsified with the adjuvant TiterMax Gold (CytRx Corp., Atlanta, GA). The antiserum was affinity-purified by absorption onto a polypeptide coupled to thiopropyl-Sepharose 6B (Amersham Biosciences Corp., Piscataway, NJ) followed by elution with 4 M $MgCl_2$. In immunoblot analysis, the antibody specifically reacted with dysferlin in microsomes of mouse skeletal muscle (data not shown). Monoclonal antibodies against dysferlin (NCL-Hamlet) and dystrophin (NCL-DYS2) were purchased from Novocastra Laboratories Ltd Newcastle, UK. Polyclonal antibody against α-actinin was obtained as described [20]. Antibodies against triadin, DHPR ($\alpha2$ subunit), ryanodine receptor and sarco/endoplasmic reticulum calcium ATPase1 (SERCA1) were obtained from Affinity Bioreagents, Inc. (Golden, CO). Antibodies against NaK-ATPase $\alpha1$ and DHPR subunit $\alpha1$ were obtained from Upstate Biotech (Lake Placid, NY). Monoclonal antibodies against annexin A2 and caveolin-3 were from BD Transduction Labs. (San Jose, CA). Anti-NSF antibody was from ICN Biomedicals, Inc. (Aurora, OH). Anti-desmin antibody was from Progen Biotechnik GMBH (Heidelberg, Germany). Goat polyclonal antibodies against DHPR $\alpha1$, SERCA1 and caveolin-3 were from Santa Cruz Biotech., Inc. (Santa Cruz, CA). The Alexa-conjugated secondary antibodies were purchased from Molecular Probes Inc. (Eugene, OR).

Immunohistochemical analysis

Animals were killed by CO_2 inhalation followed by cervical dislocation. Tibialis anterior (TA) muscles were rapidly dissected out and snap-frozen in liquid nitrogen-cooled isopentane. 6 μm thick cryostat sections were fixed by immersion in 4% paraformaldehyde in phosphate-buffered saline (PBS), pH 7.4, at 4°C for 2 min, dehydrated in 70% ethanol at 4°C for 10 min and then permeated with 0.1% triton X-100 in PBS at room temperature for 10 min. Sections were washed and incubated for 25 s with proteinase K solution (550 U/ml, Wako Pure Chemical Industries Ltd, Osaka, Japan) at a dilution of 1:300 in TE buffer [10 mM Tris-HCl (pH 8.0), 1 mM EDTA]. After washing, sections were incubated in primary antibody diluted in 2% casein in PBS at 4°C overnight. For double immunostaining, sections were incubated overnight in a mixture of the relevant primary antibodies diluted in 2% casein in PBS. After primary

135

antibody incubation, sections were washed three times for 5 min with PBS and then incubated for 1 h with the relevant secondary antibodies. After washing, sections were mounted in VectaShield® mounting medium (Vector Labs, Burlingame, CA) and coverslipped. Fluorescent images were captured by confocal-laser scanning microscope (Leica TCS SP, Leica, Heidelberg, Germany)

Subcellular membrane fractionations

Two different subcellular membrane fractionation protocols were used in the present study. The first protocol used (Fig 2A) was a slight modification of that previously reported by Dombrowski et al [21]. Briefly, muscles (~1 g) were excised from the hindlimbs of mice, cut into small pieces with scissors and frozen in liquid nitrogen. The frozen muscles were pulverized by the use of Cryo-Press chilled with liquid nitrogen and homogenized at 4°C with Polytron PT3000 equipped with a DA 3012/2S probe (Kinematica, AG, Littau Lucerne, Switzerland) at 16,000 rpm for 10 s. The original homogenizing buffer was changed to buffer A containing 20 mM sodium pyrophosphate, 20 mM sodium phosphate, 0.25 M sucrose, 0.5 mM O, O'-bis(2-aminoethyl)ethyleneglycol-N, N, N', N'-tetraacetic acid and 1 mM $MgCl_2$ (pH 7.1) in order to decrease non-specific aggregation. Discontinuous sucrose density gradient centrifugation experiments were omitted in this study.

In the second protocol (Fig 3A), sarcolemma was purified by the method of Munoz et al [22]. Homogenization steps were slightly modified as follows. Freshly dissected mouse hindlimb muscles (~6 g) were homogenized twice with a Polytron homogenizer (PT3000) at 4°C, 13,000 rpm for 20 s and centrifuged. The pellet was resuspended and again homogenized twice with the Polytron homogenizer at 17,000 rpm for 30 s. After centrifugation, the two supernatants were pooled and the remaining procedures were carried out in accordance with Munoz et al. Protease inhibitor cocktail, complete EDTA free (Roche Diagnostics GmbH, Mannheim, Germany) was included in all buffers used. All other reagents were purchased from Wako Pure Chemical.

Fractionation of microsomal proteins

Fractionation of digitonin-solubilized microsomes from rabbit skeletal muscle by wheat-germ agglutinin (WGA) gel chromatography was performed as previously described [23].

Immunoprecipitation

Besides anti-dysferlin antibody prepared in this study, anti-DHPR α1 (Upstate Biotech), anti-DHPR α2 and anti-caveolin-3 (Santa Cruz) antibodies were used for immunoprecipitation. Each IgG was coupled with the gel by use of Affi-Gel Hz immunoaffinity kit (Bio-Rad Labs, Hercules, CA). Prepared gels were washed once before use with the elution buffer: 0.15 M glycine-HCl, pH 2.5 and 0.1% digitonin before use. The WGA-bound microsomal proteins were mixed with approximately 50 µl of the gel equilibrated with the binding buffer: 0.15 M NaCl, 20 mM Hepes-NaOH, 0.1% digitonin, protease inhibitor cocktail Complete EDTA-free (Roche Diagnostics GmbH) in a MicroSpin column (Amersham Biosciences) and incubated overnight at 4°C with gentle agitation. The gel in the column was then washed many times with the binding buffer and eluted with the elution buffer. Washing and eluting procedures were performed by gravity drip from the column. The eluted proteins were neutralized with 2 M Tris-HCl, pH 9.0 and ultrafiltrated close to dehydration with Microcon 30 (Millipore Corp., Bedford, MA). The proteins were extracted from the membrane with the buffer containing 1% SDS, 1 mM TCEP (Pierce Biotechnology Inc., Rockford, IL) and 22 mM Tris-HCl (pH 6.7), and concentrated to one-third volume with a centrifugation evaporator.

Protein concentration was determined by Protein Assay Stain (Bio-Rad) or Coomassie Plus-200 Protein Assay Reagent (Pierce Biotechnology) using either BSA or γ-globulin as a standard.

Electrophoresis and Immunoblot Analysis

In SDS-PAGE, proteins were run on 5-10% or 5-15% precast gel (DRC, Tokyo, Japan). Subsequent transfer from the gel on to PVDF membranes (Millipore) was performed for 1 h at a current of 5 mA/cm^2 with a buffer similar to that of Kyhse-Anderson [24]. Following transfer, membranes were blocked with PBS including each 0.1% of casein and gelatin for 1 h at room temperature, and then incubated with primary antibodies followed by the respective horse-radish-peroxidase (HRP)-labeled secondary antibodies. Molecular masses were estimated with Biotinylated Standards kit (Bio-Rad) and HRP-labeled avidin. Bound antibodies were detected by chemiluminescence with Supersignal West Dura Extended Duration Substrate (Pierce Biotechnology). Signals were visualized with Luminoimager (Roche Diagnostics). Blot overlay assay for the

136

WGA-binding proteins was performed in accordance with the method of Yoshida and Ozawa [23]. Bound biotinyl WGA was detected with a combination of an RTU Vectastain Elite ABC reagent and a VIP-staining kit (Vector Labs).

Results

Immunohistochemical analysis of dysferlin in skeletal muscle fibers

We first analyzed the localization of dysferlin in skeletal muscles of Wistar rats and Balb/c mice by confocal laser-scanning microscopy. In both transverse and longitudinal cryosections, a mouse monoclonal antibody against dysferlin stained not only the sarcolemma but also the cytoplasm of muscle fibers (Fig. 1). In transverse sections, the cytoplasmic staining was observed as a granular staining pattern that appeared intense in some fibers. This staining pattern is similar to that previously reported [12]. In longitudinal sections, cytoplasmic localization was observed as cross-striated double bands under high magnification. We found no correlation between the intense cytoplasmic staining observed in some fibers and fiber type distribution (data not shown). We also examined the localization of dysferlin in skeletal muscles of SJL mice, which have an inframe deletion in the dysferlin gene. Dysferlin staining was significantly reduced from the sarcolemma and cytoplasm in both transverse and longitudinal sections of SJL mice skeletal muscle (Fig. 1). To investigate the specificity of the fluorescence signals observed, the antibody was also incubated with a polypeptide corresponding to its epitope. This resulted in a loss of any signal in the muscle sections (data not shown). These results indicate that dysferlin is localized not only on the sarcolemma but also within the cytoplasm of muscle fibers.

Subcellular distribution of dysferlin

Next, we examined the localization of dysferlin within muscle fibers by biochemical fractionation, using a previously established procedure [21] (Fig. 2A). This protocol allowed for the isolation of three distinct membrane fractions; a crude microsomal fraction enriched in sarcolemmal membranes (F2), and two internal membrane fractions: PF4 enriched in T-tubule and SR membranes, and PF8 an intracellular pool for glucose transporter4 (Glut4).
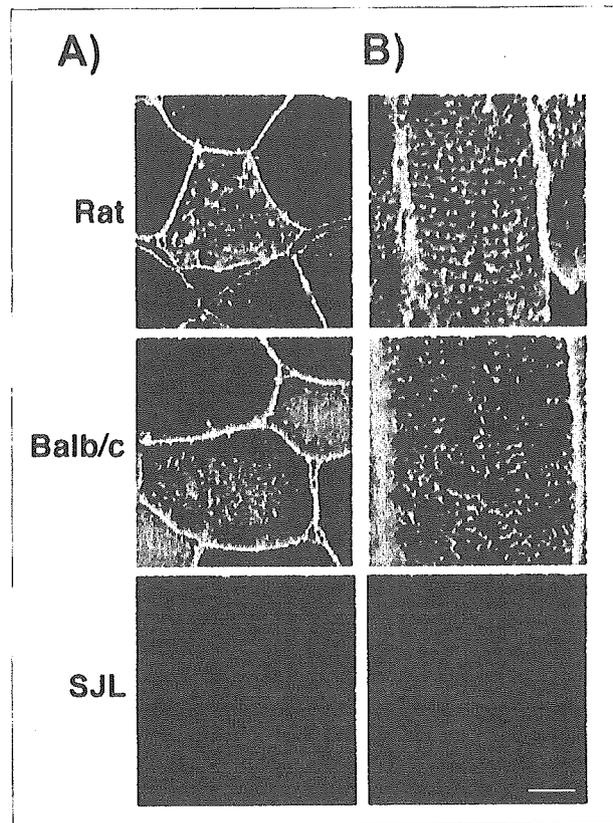

Fig. 1. Immunohistochemical analysis of dysferlin in skeletal muscle fibers. A) and B), immunofluorescent images of transverse and longitudinal sections (6 μm), respectively, of the tibialis anterior (TA) muscles of Wister rats. Balb/c and SJL mice stained with monoclonal antibody against dysferlin. Scale bar, 20 μm.

Fractions obtained from Balb/c and SJL mice were analyzed for dysferlin and a number of other protein markers (Fig. 2B). NaK-ATPase, a sarcolemmal marker, was detected only in the F2 fraction. This fraction also included annexin A2 [13] and caveolin-3 [25], two proteins reported to interact with dysferlin at the sarcolemma. On the other hand, the PF4 fraction contained the intracellular membrane proteins DHPR, SERCA1, triadin and the ryanodine receptor, although some amounts of these were also detected in the F2 fraction. As shown in Fig. 2B, dysferlin was detected not only in the sarcolemma-enriched F2 fraction, but also in the PF4 fraction. Furthermore, the intensity of the dysferlin signal was found to be similar between F2 and PF4. This result shows that a substantial amount of dysferlin distinctly associates with non-sarcolemmal membranes.
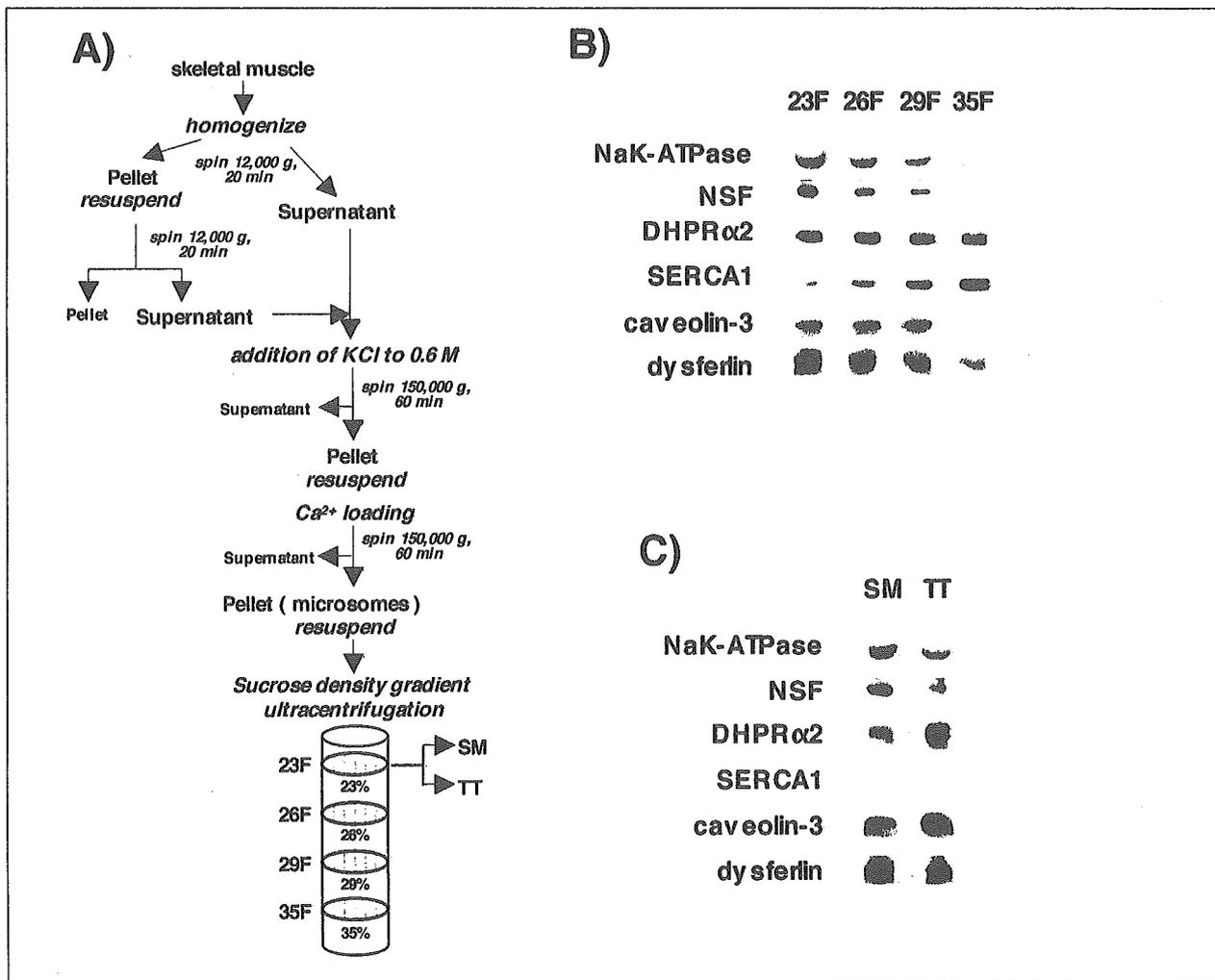
137

Fig. 2. Subcellular distribution of dysferlin in skeletal muscle. A) Schematic representation of subcellular membrane fractionation protocol [21]. F2, a crude microsomal fraction enriched in sarcolemmal membranes; PF4, internal membrane fraction enriched in T-tubule and SR membranes; PF8, internal membrane fraction enriched in GLUT4-containing intracellular membranes. B) Immunoblot analysis of the fractions obtained from Balb/c and SJL mice. Membrane proteins of each fraction were loaded on the respective lanes in equal amounts, although the amount was changed depending on the antibody used for analysis (0.05 to 5 µg). Dysferlin was detected in fractions F2 and PF4, but not in PF8. RyR, ryanodine receptor.

In the analysis of SJL mice, dysferlin was undetectable. However, we did not observe any significant changes in the amount or distribution of the other marker proteins analyzed (Fig. 2B).

Close association of dysferlin with T-tubules

The subcellular fractionation data demonstrated the presence of dysferlin in membrane fractions enriched in T-tubules and SR (Fig. 2). To further clarify the association of dysferlin with these internal membranes, we extracted crude microsomes from mouse skeletal muscle homogenates using a protocol first described by Munoz et al [22]. This crude microsomal preparation, obtained under physiological condition, includes internal membranes. This was then separated into 4 fractions based on individual densities (Fig. 3A). The lightest of these, 23F, is reportedly a fraction enriched in sarcolemma and T-tubule membranes. 26F and 29F are enriched in intracellular Glut4-containing vesicles and 35F is essentially an SR-enriched fraction [22]. Immunoblot

analysis (Fig. 3B) showed that the sarcolemmal marker, NaK-ATPase was mainly recovered in 23F, with trace amounts detected in 26F. The N-ethyl-maleimide-sensitive fusion protein (NSF), a chaperone required for the fusion of transport vesicles to their target membranes [26], displayed a similar distribution pattern to that of NaK-ATPase. SERCA1 was mainly detected in 35F and to a lesser extent in 29F, meaning most of the SR was recovered in these fractions. The T-tubule marker DHPR was detected in all fractions in the present experiment. This contrasts with the results of Munoz et al [22]. This discrepancy may be due to species differences between mice and rats. Dysferlin was mostly detected in 23F and 26F, with lesser amounts detected in 29F. The near absence of dysferlin in the SR-enriched fraction (35F) suggests that it is not likely associated with SR membranes. Caveolin-3, a dysferlin-interacting protein, was detected in fractions 23F, 26F and 29F.

Further fractionation of 23F by WGA agglutination allows for the separation of a pure sar-

138

Fig. 3. Close association of dysferlin with T-tubules. A) Schematic representation of microsomal membrane fractionation protocol [22]. 23F; light microsomal fraction enriched in sarcolemmal and T-tubule membranes, 26F and 29F; fractions enriched in Glut4-containing intracellular vesicles, 35F; an SR-enriched fraction. SM and TT; the subfractions of 23F that were agglutinated and non-agglutinated with WGA, respectively. B) Immunoblot analysis of the four microsomal fractions with various antibodies. Membrane proteins in each fraction were loaded on the respective lanes in equal amounts, with the amounts changing depending on the antibody used (0.3 to 6 µg). Dysferlin was detected in 23F and 26F, and to a lesser extent in 29F. C) Immunoblot analysis of SM and TT fractions with various antibodies. The amount of dysferlin was similar between both fractions.

colemmal fraction (SM) from a T-tubule-enriched membrane fraction (TT) [22]. This is based on the principle that WGA receptors present on T-tubules cannot interact with WGA, because of the inside-out orientation of the fragmented T-tubular membrane. As shown in Fig. 3C, NaK-ATPase and NSF were mainly detected in the SM fraction, while DHPR was mostly detected in the TT fraction. SERCA1 was notably absent from both fractions. Interestingly, dysferlin was recovered in similar amounts in both SM and TT, demonstrating that in addition to sarcolemmal localization, dysferlin closely associates with T-tubule membranes. Caveolin-3 was also detected in both fractions but comparatively more in TT.

Interaction of dysferlin with DHPR

To date, dysferlin has been reported to interact with annexins A1 & A2 [13], caveolin-3 [25] and affixin [27]. The presence of dysferlin in T-tubule-enriched intracellular membrane fractions suggests the possibility of other dysferlin-interacting proteins.

139

To investigate this possibility, we solubilized crude microsomes with digitonin and fractionated them using WGA gel affinity chromatography as depicted in Fig. 4A. As expected, dystrophin [28] and DHPR [29] were detected in the bound fraction, and proteins such as SERCA1 and NSF were detected in the flow-through fraction (Fig. 4B). Interestingly, dysferlin was detected in both fractions, indicating that a portion of dysferlin was bound to WGA. Since the amino acid sequence of dysferlin precludes it as a glycoprotein [4,5], this finding suggested to us that a portion of dysferlin may bind to WGA probably through an association with WGA-binding protein(s). Caveolin-3 was also detected in both fractions.

To find out which WGA-binding protein(s) may associate with dysferlin, we immunoprecipitated dysferlin from the bound fraction and examined the pre-cipitate for the presence of WGA-binding protein(s). Since the anti-dysferlin monoclonal antibody hitherto used was not suitable for immunoprecipitation, we raised an anti-dysferlin polyclonal antibody in rabbits as described under materials and methods. This polyclonal antibody specifically reacted with dysferlin in skeletal muscle membranes of mice (data not shown). Using this antibody, an immunoprecipitate was prepared from the WGA-bound fraction and analyzed by blot overlay assay with biotinyl WGA. As shown in Fig. 4C, positive bands were detected at approximately the 80-, 100- and 140-kDa positions. We predicted these to be putative dysferlin-interacting proteins.

DHPR, shown to bind to the WGA gel (Fig. 4B), is a protein complex composed of four subunits; α1, α2, β and γ. It reportedly binds to the gel through its
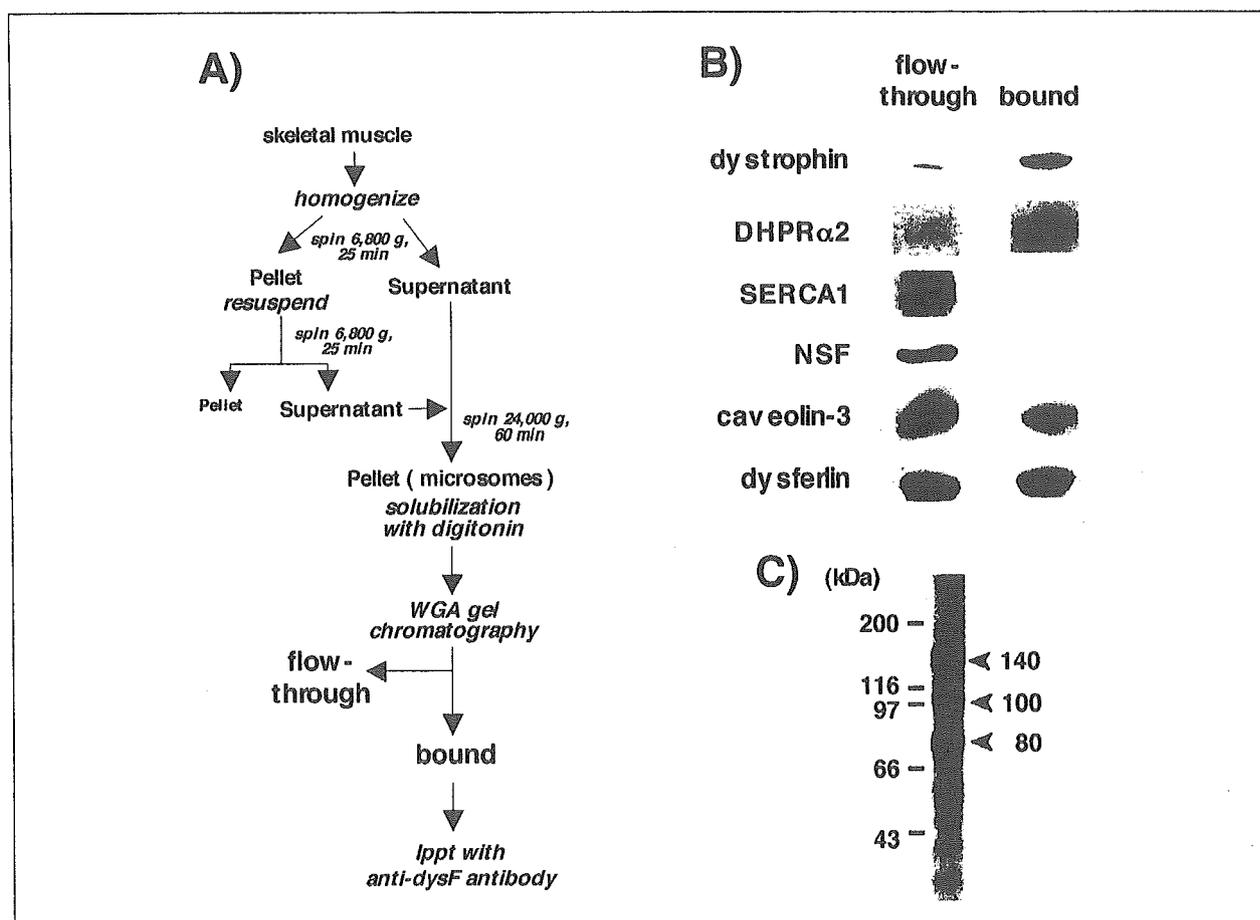
Fig. 4. Investigation of dysferlin-binding proteins. A) Schematic representation of crude microsome preparation and WGA gel chromatography of digitonin-solubilized microsomal proteins. B) Immunoblot analysis of the flow-through and bound fractions with various antibodies. The volume of both fractions was adjusted and aliquots loaded onto the gel. C) Blot overlay assay with biotinyl WGA of the immunoprecipitate prepared from the WGA-bound fraction with anti-dysferlin polyclonal antibody. Proteins of approximate molecular masses 140, 100 and 80 kDa were shown to react with WGA.

140

α2 subunit [29]. Its molecular mass of approximately 140 kDa under reduced conditions [29] is consistent with that of the largest dysferlin-interacting protein we detected (Fig. 4C). To test the possibility that dysferlin may associate with the WGA gel through an association with DHPR, we performed a series of immunoprecipitation experiments using the WGA-bound fraction. As shown in Fig. 5, DHPR was immunoprecipitated by an anti-dysferlin antibody, and conversely, dysferlin was immunoprecipitated by anti-DHPR α1 and α2 antibodies. This clearly demonstrates an interaction between dysferlin with DHPR. In another group of experiments we confirmed the presence of the dysferlin-interacting protein, caveolin-3 in immunoprecipitates prepared using the anti-dysferlin antibody. Additionally, analysis of immunoprecipitates prepared with both anti-DHPR α1 and α2 antibodies demonstrated the presence of caveolin-3, while anti-caveolin-3 antibody was found to reciprocally immunoprecipitate DHPR. These results suggest an association between DHPR and caveolin-3. Relative amounts of caveolin-3 in immunoprecipitation study indicated that only a portion of caveolin-3 might participate in the complex with dysferlin and DHPR.

We have not identified the 100- and 80-kDa WGA-binding proteins that were shown to interact with dysferlin, but their presence indicates that dysferlin may interact with more proteins than presently known.

antibodies used for

Immunoblot	Immunoprecipitation			
	anti-dysferlin	anti-DHPRα1	anti-DHPRα2	anti-caveolin-3
anti-dysferlin (McAb)	●	◦	◦	◦
anti-DHPR α2	●	●	◦	◦
anti-caveolin-3	◦	◦	◦	●

Fig. 5. Dysferlin, DHPR and caveolin-3 mutually interact. Immunoblot analysis of immunoprecipitates prepared from WGA-bound microsomal proteins. One μl of immunoprecipitates was loaded on each lane.

Partial colocalization of dysferlin with DHPR

Based on our finding that dysferlin interacts with DHPR and caveolin-3, we expect that these proteins would colocalize in skeletal muscle fibers. Therefore we set out to verify this by double immunofluorescent staining. The anti-dysferlin monoclonal and anti-DHPR α1 antibodies both produced cross-striated bands of dysferlin and DHPR, respectively, in longitudinal sections of skeletal muscle fibers (Fig. 6). Analysis of double stained patterns revealed areas of colocalization between the two proteins.

Anti-caveolin-3 antibody showed a less organized cytoplasmic staining pattern in comparison with dysferlin and DHPR, and double staining did not show clear colocalization between caveolin-3 and either DHPR (data not shown) or dysferlin. This might be explained by the notion that only a small portion of caveolin-3 associated with DHPR and dysferlin, as suggested by immunoprecipitation.

We also investigated the localization of dysferlin in relation to other well characterized sarcomeric protein markers such α-actinin and desmin, two functionally different proteins associated with Z-
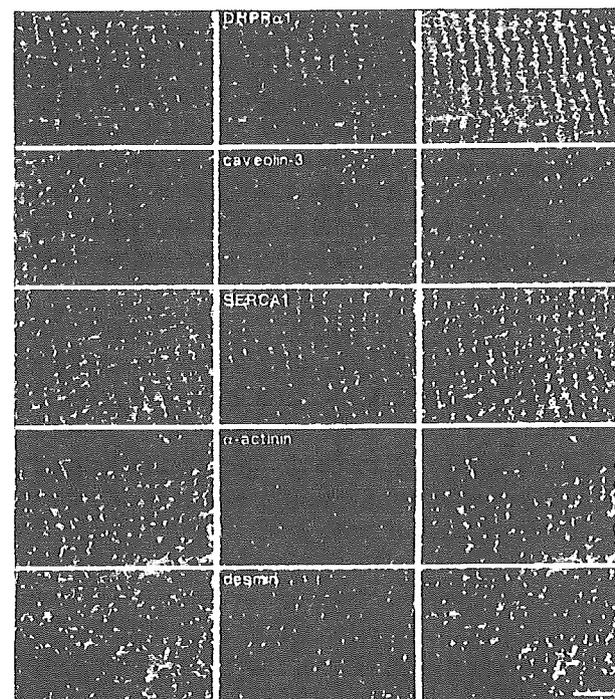

Fig. 6. Partial colocalization of dysferlin and DHPR High-resolution images of 6 μm longitudinal sections from the TA muscle of Wistar rats double stained with monoclonal antibody against dysferlin (red, left panels) and antibodies against DHPR α1, caveolin-3, SERCA1, α-actinin and desmin (green, center panels). Respective merged images are shown on the right panels. Scale bar, 5 μm.

141

lines, and SERCA1, a protein responsible for the uptake of calcium into intracellular stores. Double staining of dysferlin with either α-actinin or desmin showed no areas of colocalization. Instead, striations produced by either α-actinin or desmin were labeled within the dysferlin doublet striated pattern. Results with SERCA1 were similar to that obtained with DHPR, with comparatively fewer areas of colocalization observed.

Discussion

While no comprehensive report has been published detailing the precise localization of dysferlin within the muscle fiber, a careful examination of literature shows a consensus indicating the presence of dysferlin at both the sarcolemma [12-16] and within the cytoplasm [12,16] of muscle fibers. In the present study we confirmed the presence of dysferlin at the sarcolemma initially by immunohistochemical observation (Fig. 1). Subsequent biochemical analysis revealed the presence of dysferlin, first in a crude microsomal fraction (Fig. 2), and then in a pure sarcolemmal fraction prepared from light microsomes (Fig. 3). We also observed dysferlin localization as granular cytoplasmic staining within muscle fibers by immunohistochemistry (Fig. 1). This pattern of cytoplasmic localization was of interest in view of the fact that dysferlin has a putative role in mediating intracellular vesicle fusion with the sarcolemma [12,13]. However, since not much is known about the nature of this intracellular localization, we investigated this further via a series of biochemical experiments.

Two significant findings were made in this study. The first of these was the observation that in addition to the pure sarcolemmal fraction, a portion of dysferlin was present in a T-tubule-enriched intracellular membrane fraction (Fig. 3). This was determined using a protocol of subcellular fractionation with further purification by WGA agglutination. T-tubules are specialized membrane invaginations of the sarcolemma and carry membrane depolarization deep into the fiber to trigger excitation-contraction coupling [30]. The protein and lipid composition of this system has been shown to be very distinct from that of the sarcolemma [30]. This suggests that the association of dysferlin with T-tubules may be independent of its localization at the sarcolamma, and is the first published data describing an association of dysferlin with non-sarcolemmal membranes.

Another significant finding was the identification of DHPR as a dysferlin-interacting protein complex. This result supports the finding of dysferlin present on T-tubules. The DHPR is responsible for the L-type Ca^{2+} current and serves as the voltage sensor for excitation contraction coupling [32]. It is composed of α1, α2, β and γ subunits [29]. The α1 subunit is a transmembrane protein that contains the basic functional elements for the L-type Ca^{2+} channel while the β subunit is an intracellular protein essential for excitation contraction coupling. The functional significance of the α2 and γ subunits is not clearly defined [32].

The question remains as to exactly how dysferlin associates with DHPR. Two possibilities exist as to how dysferlin may interact with DHPR. One involves a lateral association between dysferlin and DHPR in T-tubule membranes. The other involves an association between dysferlin, present in intracellular vesicles, and DHPR. Double immunostaining (Fig. 6) and membrane fractionation experiments indicate that the entire DHPR complex may not interact with dysferlin. Therefore, we are of the opinion that the interaction occurs between dysferlin and DHPR present on distinct membranes respectively.

It is not clear whether this association is direct or not, but it is interesting to assume that some other protein(s) may be involved in this association. The WGA-binding proteins of molecular masses 80 and 100 kDa shown to interact with dysferlin (Fig. 4C) might be involved in this association. Alternatively, caveolin-3, reported to be dysferlin-interacting protein [25] might be involved. In the present study, we observed by biochemical analysis that caveolin-3 associated with both membranes of T-tubules and the sarcolemma (Fig. 3). This distribution pattern was consistent with previous reports [33]. We confirmed by immunoprecipitations that dysferlin in fact interacts with caveolin-3 and in addition, we found that caveolin-3 interacts with DHPR. These results show that dysferlin, DHPR and caveolin-3 may participate in the formation of a large oligomeric complex. Caveolin-3 is a major protein component of cardiac and skeletal muscle caveolae [34], another system of specialized membrane invaginations of the sarcolemma implicated in a number of cellular processes including calcium homeostasis [35] and signal transduction [36]. It has been suggested that caveolin-3 associates mainly with T-tubules during myogenesis and has been proposed to play a role in the formation of T-tubules [37]. Indeed, caveolin-3 knockout mice show a phenotype

142

with T-tubule abnormalities [38], but most of caveolin-3 in the adult stage has been found at the sarcolemma by immunohistochemistry [37]. Caveolin-3 has also been reported to participate in an insulin-regulated transport mechanism in muscle [33]. Under activation, caveolin-3-containing vesicles traffic between intracellular sites and target sites on the sarcolemma and T-tubules. Not much is known about the precise nature of how caveolin-3 associates with T-tubules. However, based on our finding, it would be intriguing to assume that dysferlin might be involved in the fusion of caveolin-3-containing vesicles with T-tubules.

On the basis of immunohistochemical finding that dysferlin is present in the cytoplasm [12,16], it has been proposed that dysferlin-carrying vesicles participate in the injury-induced membrane repair of the sarcolemma [17]. However, our present findings suggest that the cytoplasmic staining does not always show the presence of such vesicles, since at least a portion was contributed by T-tubule-associated dysferlin. Evaluation of the proposed model, together with identification of the dysferlin-carrying membrane vesicles, should be encouraged by further studies.

In conclusion, we have shown by systematic subcellular membrane fractionation that dysferlin associates with both sarcolemma- and T-tubule-enriched membrane fractions. The latter was consistent with our demonstrated interaction of dysferlin with DHPR. We have also shown an association between DHPR and the dysferlin-interacting protein caveolin-3, raising the possibility that dysferlin may form an oligomeric complex. Two not yet identified WGA-binding proteins, 80 and 100 kDa, may participate in this complex. Our findings suggest that dysferlin might play role(s) other than the putative injury-induced membrane repair.

Acknowledgements

Abbreviations

C. elegans, Caenorabditis elegans; DHPR, the dihydropyridine receptor; EGTA, O, O'-bis(2-aminoethyl)ethyleneglycol-N, N, N', N'-tetraacetic acid; LGMD 2B, limb girdle muscular dystrophy 2B; NaK-ATPase, sodium potassium ATPase; RyR, ryanodine receptor; SR, the sarcoplasmic reticulum; T-tubules, transverse tubules; SERCA, sarco/endoplasmic reticulum calcium ATPase; WGA, wheat germ agglutinin.

References

1. Miyoshi K, Kawai H, Iwasa M, et al. Autosomal recessive distal muscular dystrophy as a new type of progressive muscular dystrophy. Seventeen cases in eight families including an autopsied case. Brain 1986;109:31–54.
2. Bashir R, Strachan T, Keers S, et al. A gene for autosomal recessive limb-girdle muscular dystrophy maps to chromosome 2p. Hum Mol Genet 1994;3:455-7.
3. Galassi G, Rowland LP, Hays AP, et al. High serum levels of creatine kinase: asymptomatic prelude to distal myopathy. Muscle Nerve 1987;10:346-50.
4. Liu J, Aoki M, Illa I, et al. Dysferlin, a novel skeletal muscle gene, is mutated in Miyoshi myopathy and limb girdle muscular dystrophy. Nature Genet 1998;20:31-6.
5. Bashir R, Britton S, Strachan T, et al. A gene related to Caenorhabditis elegans spermatogenesis factor fer-1 is mutated in limb-girdle muscular dystrophy type 2B. Nature Genet 1998;20:37-42.
6. Rizo J, Sudhof TC. C2 domains, structure and function of a universal binding domain. J Biol Chem 1998;273:15879-82.
7. Li C, Ullrich B, Zhang JZ, et al. Ca(2+)-dependent and -independent activities of neural and non-neural synaptotagmins. Nature 1995; 375: 594-9.
8. Perin MS, Fried VA, Mignery GA, et al. Phospholipid binding by a synaptic vesicle protein homologous to the regulatory region of protein kinase C. Nature 1990; 345: 260-3.
9. Davis DB, Delmonte AJ, Ly CT, et al. Myoferlin, a candidate gene and potential modifier of muscular dystrophy. Hum Mol Genet 2000;9:217-26.
10. Yasunaga S, Grati M, Cohen-Salmon M, et al. A mutation in OTOF, encoding otoferlin, a FER-1-like protein, causes DFNB9, a nonsyndromic form of deafness. Nature Genet. 1999; 21: 363-9.
11. Achanzar WE, Ward S. A nematode gene required for sperm vesicle fusion. J Cell Sci 1997;110:1073-81.
12. Bansal D, Miyake K, Vogel SS, et al. Defective membrane repair in dysferlin-deficient muscular dystrophy. Nature 2003;423:168-72.
13. Lennon NJ, Kho A, Bacskai BJ, et al. Dysferlin interacts with annexins A1 and A2 and mediates sarcolemmal wound-healing. Biol. Chem. 2003;278:50466-73.
14. Anderson LV, Davison K, Moss JA, et al. Dysferlin is a plasma membrane protein and is expressed early in human development. Hum Mol Genet 1999;8:855-61.

143

15. Matsuda C, Aoki M, Hayashi YK, et al. Dysferlin is a surface membrane-associated protein that is absent in Miyoshi myopathy. Neurol 1999;53:1119-22.

16. Piccolo F, Moore SA, Ford GC, et al. Intracellular accumulation and reduced sarcolemmal expression of dysferlin in limb-girdle muscular dystrophies. Ann Neurol. 2000;48:902-12.

17. Bansal D, Campbell KP. Dysferlin and the plasma membrane repair in muscular dystrophy. Trends Cell Biol 2004;14:206-13.

18. Bittner RE, Anderson LVB, Burkhardt E, et al. Dysferlin deletion in SJL mice (SJL-Dysf) defines a natural model for limb girdle muscular dystrophy 2B. Nature Genet 1999;23:141-2.

19. Vafiadaki E, Reis A, Keers S, et al. Cloning of the mouse dysferlin gene and genomic characterization of the SJL-Dysf mutation. Neuroreport 2001;12:625-9.

20. Tokuue Y, Goto S, Imamura M, et al. Transfection of chicken skeletal muscle α-actinin cDNA into nonmuscle and myogenic cells: dimerization is not essential for α-actinin to bind to microfilaments. Exp Cell Res 1991;197:158-67.

21. Dombrowski L, Roy D, Marcotte B, et al. A new procedure for the isolation of plasma membranes, T tubules, and internal membranes from skeletal muscle. Am J Physiol 1996;270:E667-76.

22. Munoz P, Rosemblatt M, Testar X, et al. Isolation and characterization of distinct domains of sarcolemma and T-tubules from rat skeletal muscle. Biochem J 1995; 307:273-80.

23. Yoshida M, Ozawa E. Glycoprotein complex anchoring dystrophin to sarcolemma. J Biochem 1990;108:748-52.

24. Kyhse-Anderson J. Electroblotting of multiple gels: a simple apparatus without buffer tank for rapid transfer of proteins from polycrylamide to nitrocellulose J Biochem Biophys Methods.1984;10:203-9.

25. Matsuda C, Hayashi YK, Ogawa M, et al. The sarcolemmal proteins dysferlin and caveolin-3 interact in skeletal muscle. Hum Mol Genet 2002;10:1761-6.

26. Jahn R, Sudhof TC. Membrane fusion and exocytosis. Annu Rev Biochem 1999;68:863-911.

27. Matsuda C, Kameyama K, Tagawa K, et al. Dysferlin interacts with affixin (beta-parvin) at the sarcolemma. J Neuropathol Exp Neurol 2005;64:334-40.

28. Ervasti JM, Ohlendieck K, kahl SD, et al. Deficiency of a glycoprotein component of the dystrophin complex in dystrophic muscle. Nature 1990;345:319-25.

29. Campbell KP, Leung AT, Sharp AH. The biochemistry and molecular biology of the dihydropyridine-sensitive calcium channel. Trends Neurosci 1988;11:425-30.

30. Flucher BE. Structural analysis of muscle development: transverse tubules, sarcoplasmic reticulum, and the triad. Dev Biol 1992;154:245-60.

31. Ursu D, Sebille S, Dietze B, et al. Excitation-contraction coupling in skeletal muscle of a mouse lacking the dihydropyridine receptor subunit gamma1. J Physiol 2001;533:367-77.

32. Ahern CA, Vallejo P, Mortenson L, et al. Functional analysis of a frame-shift mutant of the dihydropyridine receptor pore subunit (alpha1S) expressing two complementary protein fragments. BMC Physiol 2001;1:1-11.

33. Munoz P, Mora S, Sevilla L, et al. Expression and insulin-regulated distribution of caveolin in skeletal muscle. Caveolin does not colocalize with GLUT4 in intracellular membranes. J Biol Chem 1996;271:8133-9.

34. Rothberg KG, Heuser JE, Donzell WC, et al. Caveolin, a protein component of caveolae membrane coats. Cell 1992;68:673-82.

35. Fujimoto T. Calcium pump of the plasma membrane is localized in caveolae. J Cell Biol 1993;120:1147-57.

36. Lisanti MP, Scherer PE, Tang Z, et al. Caveolae, caveolin and caveolin-rich membrane domains: a signaling hypothesis. Trends Cell Biol 1994;4:231-35.

37. Parton RG, Way M, Zorzi N, et al. Caveolin-3 associates with developing t-tubules during muscle differentiation. J Cell Biol 1997;136:137-54.

38. Galbiati F, Engelman JA, Volonte D, et al. Caveolin-3 null mice show a loss of caveolae, changes in the microdomain distribution of the dystrophin-glycoprotein complex, and T-tubule abnormalities. J Biol Chem 2001;276:21425-33.

144

Major clinical and histopathological characteristics of canine X-linked muscular dystrophy in Japan, CXMDJ

Yoshiki Shimatsu[1], Madoka Yoshimura[1], Katsutoshi Yuasa[1],
Nobuyuki Urasawa[1], Masayuki Tomohiro[1], Masao Nakura[2], Manabu Tanigawa[2],
Akinori Nakamura[1], Shin'ichi Takeda[1]

[1]*Department of Molecular Therapy, National Institute of Neuroscience,*
National Center of Neurology and Psychiatry, 4-1-1 Ogawa-higashi, Kodaira, Tokyo 187-8502, Japan
[2]*Chugai Research Institute for Medical Science, Inc., 6598 Toyoda, Suwa, Nagano 392-0016, Japan*

Canine X-linked muscular dystrophy (CXMD), which was found in a colony of golden retriever, is caused by a mutation in the *dystrophin* gene and it is a useful model of Duchenne muscular dystrophy (DMD). To investigate the pathogenesis and to develop therapy of DMD, we have established a beagle-based CXMD colony in Japan (CXMDJ) and examined their phenotypes. The mortality by 3 days of age in the third generation (G3) of CXMDJ dogs, 32.3%, was considerably higher than that in normal G3 littermates, 13.3%. Serum creatine kinase (CK) levels of G3 CXMDJ were significantly higher than that of normal male dogs with two peaks: at shortly after birth and around 2 months of age. Diaphragm muscle involvement occurred shortly after birth and was more severe than that of limb muscles. Stress during whelping might be associated with the neonatal death and respiratory muscle involvement. Gait disturbance was also noticed after 2 months of age. The involvement of limb and temporal muscles was observed from 2 months of age, which corresponded with the second peak of serum CK. Macroglossia, dysphagia, drooling and jaw joint contracture were overt from 4 months of age. We noticed severe macroglossia and hypertrophy of the sublingual muscles at the age of 12 months, and these were important features of this model, because dysphagia is one of major symptoms in older DMD patients. Overall, the phenotypes of CXMDJ were roughly identical to those of CXMD dogs in the literature. Beagle-based CXMDJ is smaller and easier to handle than golden retriever, therefore they are a useful model for DMD.

Key words: Canine X-linked muscular dystrophy; dystrophin; creatine kinase

Introduction

Duchenne muscular dystrophy (DMD) is an X-linked recessive disease characterized by skeletal muscle atrophy and weakness [1], and is caused by mutations in the *dystrophin* gene [2]. DMD patients exhibit muscle weakness by 2 to 5 years of age, are unable to walk, and die by their twenties as a result of either respiratory or cardiac failure [1]. Recently the prognosis of patients suffering from DMD has been greatly improved by the use of respirators.

In research on the molecular pathogenesis of dystrophin deficiency, *mdx* mice have been frequently used as an experimental model, but the clinical symptoms of *mdx* mice are much milder than those of patients suffering from DMD [3]. Another model for DMD, canine X-linked muscular dystrophy (CXMD), which was found in a golden retriever, lacks dystrophin, and reveals clinical and pathological findings that are more similar to those of DMD [4-7]. Therefore, CXMD dogs are more appropriate than *mdx* mice as an animal model [5, 7, 8], although a severely affected animal model is difficult to raise and handle.

We established a beagle-based colony of CXMD dogs in Japan designated CXMDJ [9]. The first generations (G1) of carrier female dogs were produced by artificial insemination of a beagle bitch with frozen semen derived from a CXMD, and the second generation (G2) and the third generation (G3) of CXMDJ dogs were born to interbreed G1 and G2 carrier female dogs and beagle sires, respectively.

CXMD is a very important experimental model for the development of therapies for dystrophin deficiency. The efforts that have been made to

145

explore experimental therapies in *mdx* mice may also be applicable to a large animal model such as CXMD in the future. These efforts include pharmaceuticals [10], gene transfer [11], or cell transplantation therapy [12]. Very recently hematopoietic cell transplantation has been tried using CXMD [13]. In this report, the major phenotypes of G3 CXMD$_J$ dogs were investigated and compared with those of CXMD dogs. We found that CXMD$_J$ dogs are a suitable model to develop therapies for DMD.

Materials and Methods

Animals

All dogs were part of the CXMD$_J$ breeding colony at the General Animal Research Facility, National Institute of Neuroscience, National Center of Neurology and Psychiatry (Tokyo, Japan) or Chugai Research Institute for Medical Science, Inc. (Nagano, Japan) [9]. Seven G2 carrier females were mated with normal beagle sires or inseminated with fresh normal beagle semen. Ninety-nine G3 pups were produced by 12 whelpings of G2 carriers. The genotypes of the pups were analyzed by Snapback SSCP [14]. Forty-five male and female littermates were normal, 31 male pups were affected, and 23 female pups were carriers. We analyzed affected G3 males together with normal G3 male and female littermates, and carrier G3 females in this study.

A pregnant carrier G2 female was removed to stainless steel cage for whelping (1,580 x 1,580 x 930 mm) at 7 days before the expected whelping day. The carrier female nursed G3 pups after her whelping, and the weaning of pups was done at 6 weeks after birth. Affected G3 pups were then individually housed in the cages (1,700 x 960 x 1,570 mm), but the remaining pups were fed with 2 or 3 pups in the same largeness of cages up to around 3 months of age. All dogs were given a mixture of soaking pellet with synthetic powdered milk up to 3 months of age, and then given a pellet diet. They also had *ad libitum* access to filtered water. The room temperature was maintained at 22 ± 2°C, and the relative humidity was 40-70%. A veterinarian examined the healthy care of the dogs once a week. All dogs in this experiment were treated in accordance with the guidelines provided by the Ethics Committee for Treatment of Laboratory Middle-Sized Animals of the National Institute of Neuroscience, National Center of Neurology and Psychiatry (Tokyo, Japan) or the Ethics Committee for Treatment of Laboratory Animals of Chugai Pharmaceutical Co., Ltd. (Tokyo, Japan).

Death by 3 days of age

The rates of death by 3 days of age were calculated in 31 affected G3 male pups and 45 normal G3 male and female pups, respectively.

Body weight

The body weight of normal (n = 4) and affected (n = 8) G3 males were measured at every second day from 1 to 21 days, and at 1.5, 2, 4, 6, 8, 10, and 12 months of age. Synthetic milk was given through tube for 14 days to four affected G3 pups whose body weight at 3 days of age was decreased than that of 1 day after birth.

Serum creatine kinase (CK) levels

Blood samples of normal male (n = 5), female (n = 3 before 2 months of age, n = 2 at 3 months of age), affected male (n = 8), and carrier female (n = 4) G3 dogs were obtained by cephalic or jugular venipuncture at 1 day, 3 weeks, and 1.5, 2, 3, 6, and 12 months of age. Serum CK levels were assayed using an automated colorimetric analyzer (FDC3500, FujiFilm Medical, Tokyo, Japan).

Clinical manifestations

We observed gait and mobility disturbances, involvement of limb, temporal, and tongue muscles, dysphagia, and drooling as clinical signs in normal (n = 5) and affected (n = 5) G3 males at the ages of 1, 2, 4, 6, and 12 months. The severity of each sign was classified according to a new grading scale for the CXMD$_J$ colony (Table) based on both a previous report [15] and a clinical record prepared for an Australian CXMD colony by J.M. Howell et al. (personal communication). We also measured the maximum mouth opening to evaluate the jaw joint contracture. At least one veterinarian and two medical doctors who are very familiar with symptoms of dystrophic dogs did all clinical examinations.

Macroscopic and histopathological examinations

Muscle samples from normal (n = 5) and affected (n = 5) G3 males were obtained when

146

Table 1. Grading of clinical signs in CXMDᴊ dogs.

```
Gait disturbance
       Grade   1: None
       Grade   2: Sitting with hind legs extended
       Grade   3: Bunny hops with hind legs
       Grade   4: Shuffling walk
       Grade   5: Unable to walk

Mobility disturbance
       Grade   1: None
       Grade   2: lying down more than normal
       Grade   3: Cannot jump on hind legs
       Grade   4: Increasing difficulty moving around
       Grade   5: Unable to get up and move around

Limb or temporal muscle atrophy
       Grade   1: None
       Grade   2: Suspect hardness
       Grade   3: Can feel hardness or apparently thin
       Grade   4: Between Grade 3 and 5
       Grade   5: Extremely thin or hard

Drooling
       Grade   1: None
       Grade   2: Occasionally dribbles saliva when sitting
       Grade   3: Some drool when eating and drinking
       Grade   4: Strings of drool when eating or drinking
       Grade   5: Continuous drool

Macroglossia
       Grade   1: None
       Grade   2: Slightly enlarged
       Grade   3: Extended outside dentition
       Grade   4: Enlarged and slightly thickened
       Grade   5: Enlarged and thickened

Dysphagia
       Grade   1: None
       Grade   2: Takes time and effort in taking food
       Grade   3: Difficulty in taking food from plate
       Grade   4: Difficulty in chewing, swallowing or drinking
       Grade   5: Unable to eat
```

These grading scales were developed at our institute on the basis of a previous report [15] and a personal communication with J.M. Howell et al. in Australia.

the dogs died at 1 day of age or were sacrificed at the ages of 3 days and 2, 6, and 12 months by using an overdose of intravenous pentobarbital. Some portions of the diaphragm and anterior tibial muscles were snap-frozen in cooled isopentane, and cryostat sections (6 μm) were stained with hematoxylin and eosin (H&E). The tongue, genioglossus, and geniohyoideus muscles were fixed in 15% neutral buffered formalin, embedded in paraffin, and 6 μm sections were stained with H&E.

Statistical analysis

The data of body weight, serum CK level, and the maximum mouth opening were subjected to a one-way analysis of variance test. Fisher's protected least significant difference test was used for post-hoc comparisons. The statistical significance of the pup death rate was evaluated using the chi-square test. All values are expressed as mean ± standard error (S.E.). A p value of less than 0.05 was considered to indicate statistical significance. All calculations were performed using StatView software (SAS Institute, Cary, NC, USA).

Results

Death by 3 days of age

Ten of 31 G3 CXMDᴊ pups died, a death rate of 32.3%. Among normal G3 male and female pups, six out of 45 (13.3%) died. The ratio of affected G3 pups was significantly higher than that of normal pups ($p < 0.05$). We did not find any dead pups from 4 days to 4 weeks of age during the lactation period.

Body weight

Body weight changes of G3 male dogs (4 normal and 4 affected without tube feeding) in the CXMDᴊ colony are shown in **Fig. 1A**. Affected G3 males showed retardation in increase of body weight after 6 months of age and the difference between them was statistically significant at the age of 10 and 12 months (**Fig. 1A**). While, the body weight of affected G3 male pups needed tube feeding was significantly lower than that of either normal or affected G3 male without tube feeding at 5, 7, and 9 days of age (**Fig. 1B**). The difference in body weight between normal and carrier G3 females was not seen from 1 day to 6 months of age (data not shown).

Serum CK levels

Changes of serum CK levels of dogs in the CXMDᴊ colony are shown in **Fig. 2**. The values of normal G3 males and females ranged from 80 to 4,000 IU/l up to 12 months of age. The difference in the CK levels between normal and affected G3 males was statistically significant at every age examined. The average serum CK level made a biphasic pattern: it was 120,000 IU/l at 1 day of age and then had decreased to 11,000 IU/l at 3
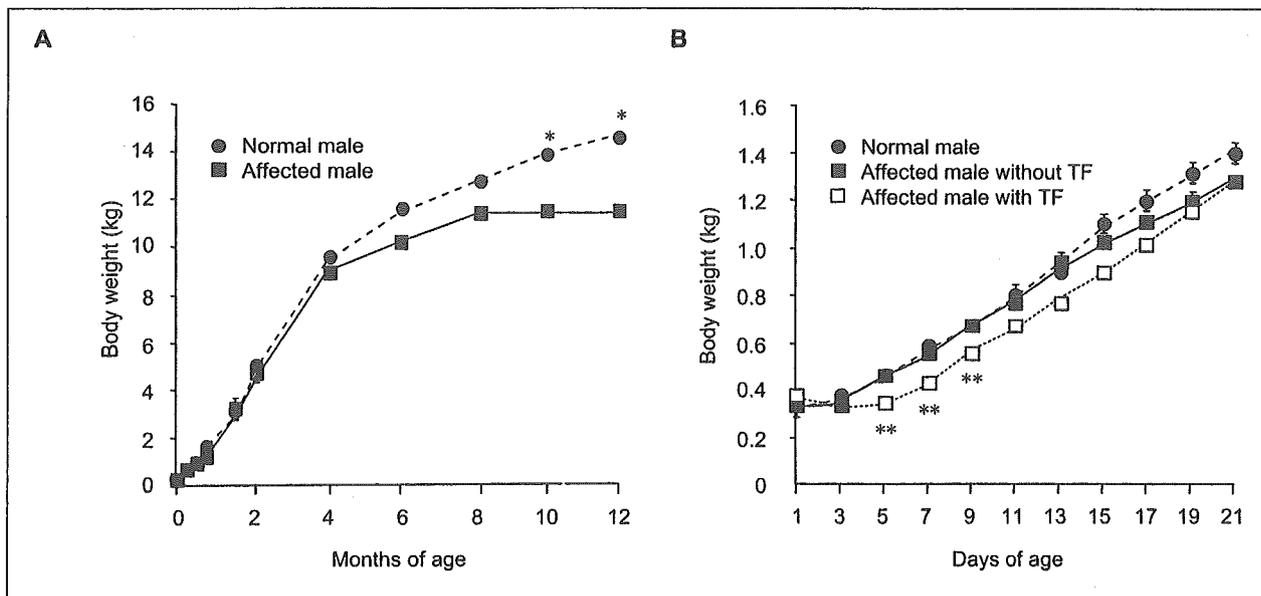
147

Figure 1. (A) Body weight changes up to 12 months of normal and affected G3 male dogs in CXMDj colony. (B) Body weight changes of G3 male dogs of normal, affected without tube feeding (TF), and affected with TF up to 21 days. Bar: mean ± S.E.; $**p < 0.01$; $*p < 0.05$.
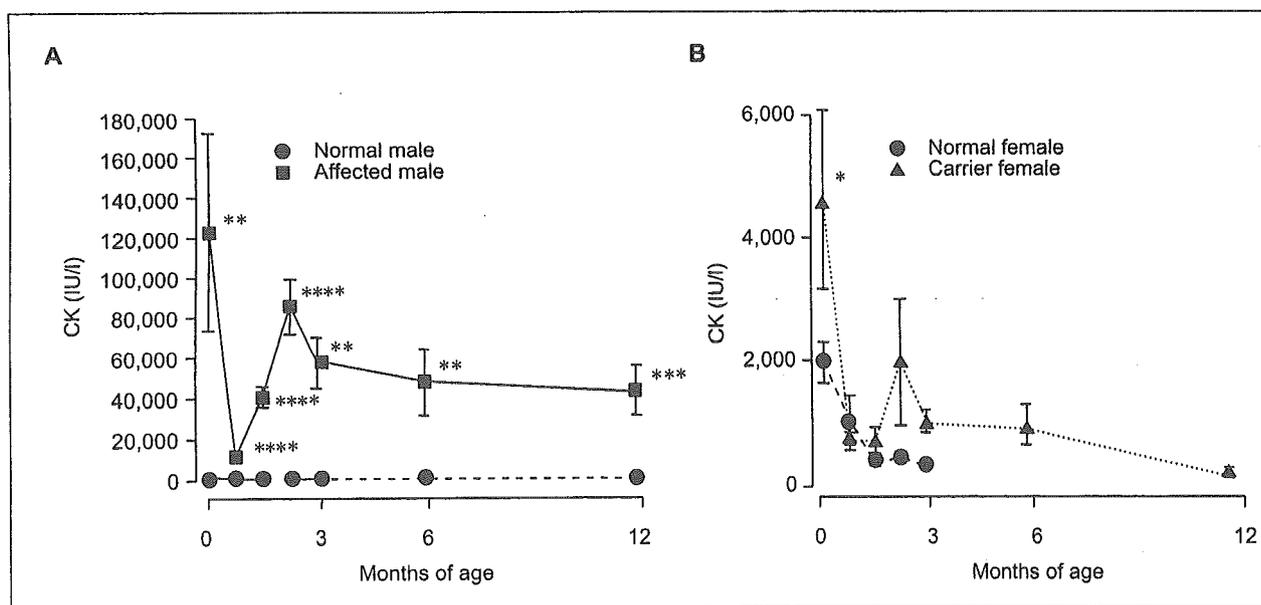

Figure 2. Serum CK levels of G3 dogs in CXMDj colony in (A) normal and affected males and (B) normal and carrier females. Bar: mean ± S.E.; $****p< 0.0001$; $***p < 0.001$; $**p < 0.01$; $*p < 0.05$.

weeks of age (**Fig. 2A**); however, the levels had increased again to 85,000 IU/l at 2 months of age, and then the values gradually decreased. Like affected G3 males, the serum CK levels in carrier G3 females, both at 1 day and 2 months of age, were higher than those in normal G3 females, and the difference at 1 day of age was statistically significant (**Fig. 2B**).

Clinical manifestations

In CXMD male dogs at 14 months of age, kyphosis and atrophy of temporal, truncal, and limb muscles were observed; many muscles, especially the proximal limb muscles, were firm on palpation [15]. A representative G3 CXMDj male dog at 12 months of age had signs similar to those described above (**Fig. 3**). Moreover, CXMD dogs
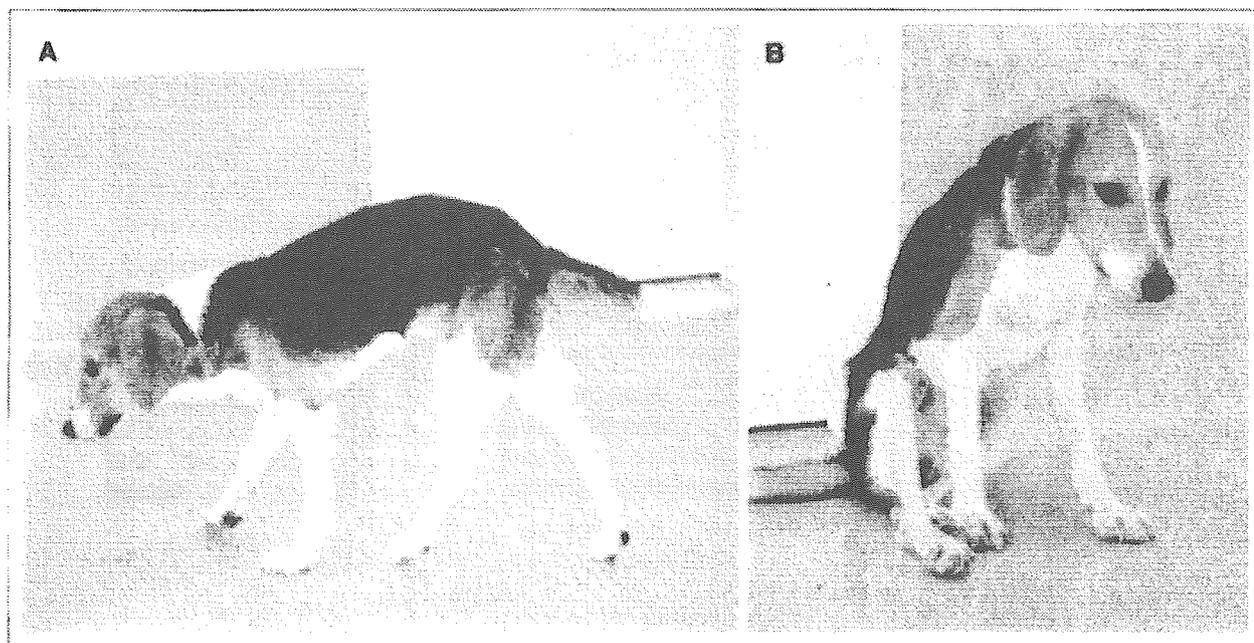
148

Figure 3. A representative affected G3 male dog at 12 months of age.
(**A**) When walking, spine curvature, supinate front paws, and drop feet in hind limbs were observed.
(**B**) Severe temporal muscle atrophy and throwing of hind limbs when sitting were recognized.

showed gait and mobility disturbances, and progressive tongue enlargement, dysphagia, feeding difficulty, and excessive salivation were also recognized [15]. We, therefore, evaluated the clinical phenotypes of affected G3 male dogs at the ages of 1, 2, 4, 6, and 12 months.

Within a week after the birth, affected pups were slightly less active than normal littermates during the period. Around 2 months of age, dystrophic pups sometimes sit with hind legs extended. The dog showed stiff limbs, but these symptoms were probably related to contraction of the joints. Soon after, they move the hind limbs simultaneously (bunny-hops with hind legs) (**Fig. 4A and B**). Distal limb muscle atrophy appeared from 2 months of age in the dogs (**Fig. 4C**), but proximal limb muscle atrophy in G3 males was observed at 4 months of age (**Fig. 4D**). Proximal limb muscle, especially thigh muscle, has been spared at the relatively early period, but that was severer than distal limb muscle atrophy at 12 months of age (**Fig. 3A**). The temporal muscle was also involved at the age of 2 months, and it was much more atrophied than other muscles at the age of 12 months (**Fig. 3B and 4E**). Around 4 months of age, they occasionally dribbled saliva when sitting. They frequently showed tongue hypertrophy (**Fig. 4F and G**), and inability to open

the jaw due to contracture of the joints. 40% of dogs showed difficulty in eating food or swallowing at the age of 6 months (**Fig. 4H**), therefore hand feeding is sometimes required for the dogs. An enlarged and thickened tongue was seen in all affected G3 males at 12 months of age. To ascertain the degree of jaw joint contracture, we examined the maximum mouth opening in both normal and affected G3 males (**Fig. 4I**). The extent of the opening in normal G3 males increased with age, but it did not change much in the affected G3 dogs. The difference between them was significant at 4, 6, and 12 months of age, therefore jaw joint contracture probably started around 4 months of age in G3 affected dogs.

Macroscopic and histopathological findings

The diaphragm muscle of a normal G3 male that died at 1 day of age did not show streaks in the muscular portions (**Fig. 5A**); however, there were many radiating white streaks in an affected G3 male that died at 1 day of age (data not shown) as well as in another affected G3 male that was sacrificed at 3 days of age (**Fig. 5D**). Histopathological examination of the diaphragm muscle in a sacrificed, affected G3 male at 3 days of age showed acute stage of diffuse muscle necrosis with edema (**Fig. 5E**). At the age of 6 months, the
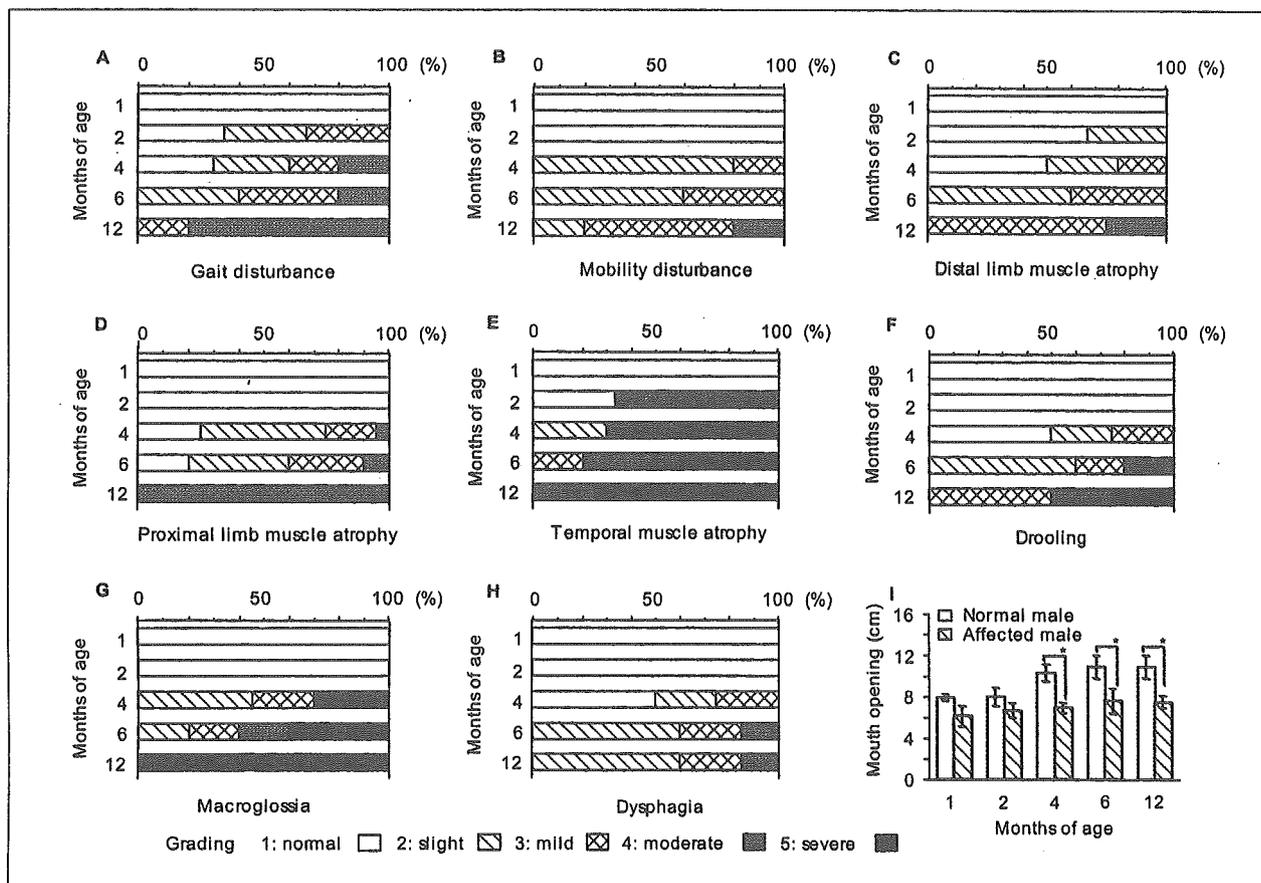
149

Figure 4. Evaluation of clinical phenotypes in affected G3 male dogs. The evaluation of each clinical sign is shown in A-H: (A) gait disturbance, (B) mobility disturbance (C) distal limb, (D) proximal limb, (E) and temporal muscle atrophy, (F) drooling, (G) macroglossia, and (H) dysphagia at the ages of 1, 2, 4, 6, and 12 months. The severity of each sign in affected G3 dogs was classified into five grades as described in Materials and Methods and Table. The percentage of affected G3 dogs in each grade was calculated for each month of age. (I) Maximum mouth opening in normal and affected G3 male dogs at the ages of 1, 2, 4, 6, and 12 months. Bar: mean ± S.E.; $*p < 0.05$.

diaphragma muscle in an affected G3 male disclosed marked variation in fiber size and increase in fibrosis and necrotic fibers (Fig. 5F).

The diameter of the fibers in the anterior tibial muscle increased with age in normal G3 males (Fig. 6A-C), while the muscle in the sacrificed, affected G3 male at 3 days of age showed slight fiber size variation and some necrotic fibers (Fig. 6D). The findings were not different from those in an affected G3 male that died at 1 day of age (data not shown). At the age of 2 months, the tibial muscle from an affected G3 male displayed an increase in the number of necrotic fibers, invasion of inflammatory cells, and a slight proliferation of the interstitial tissues (Fig. 6E). At the age of 6 months, marked fiber size variation, increase in the interstitial fibrosis, and hypertro-

phied or centrally nucleated fibers were observed (Fig. 6F).

In macroscopic examinations, an affected G3 male at the age of 12 months had severe hypertrophy of the tongue, genioglossus, and geniohyoideus muscles (Fig. 7B) as compared with those in a normal male (Fig. 7A). In the tongue muscle, there were many hypertrophied fibers and opaque fibers (Fig. 7D), as compared with those in the normal male (Fig. 7C).

Discussion

In this report, we described the major clinical and histopathological phenotypes of beagle-based dystrophic dogs, CXMDj, that carried the same *dystrophin* gene mutation as CXMD dogs. We
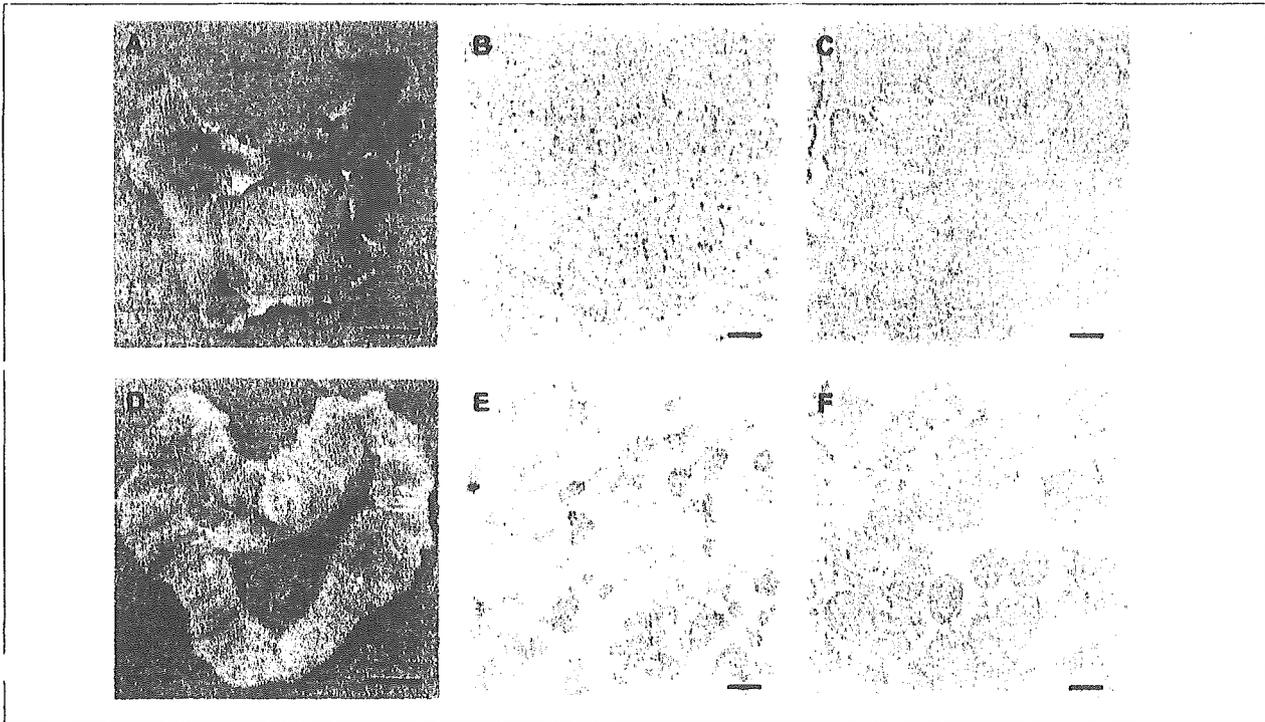
150

Figure 5. Macroscopy and histopathology of diaphragm muscles. Diaphragm of a normal G3 male dog that died at 1 day of age (**A**) and an affected G3 male dog that was sacrificed at 3 days of age (**D**). Bar = 1 cm. H&E staining of cross-sections of diaphragm muscles from normal G3 male at 3 day of age (**B**) and at 6 months of age (**C**), and from affected G3 males that was sacrificed at 3 days of age (**E**) and 6 months of age (**F**). Bar = 50 μm.
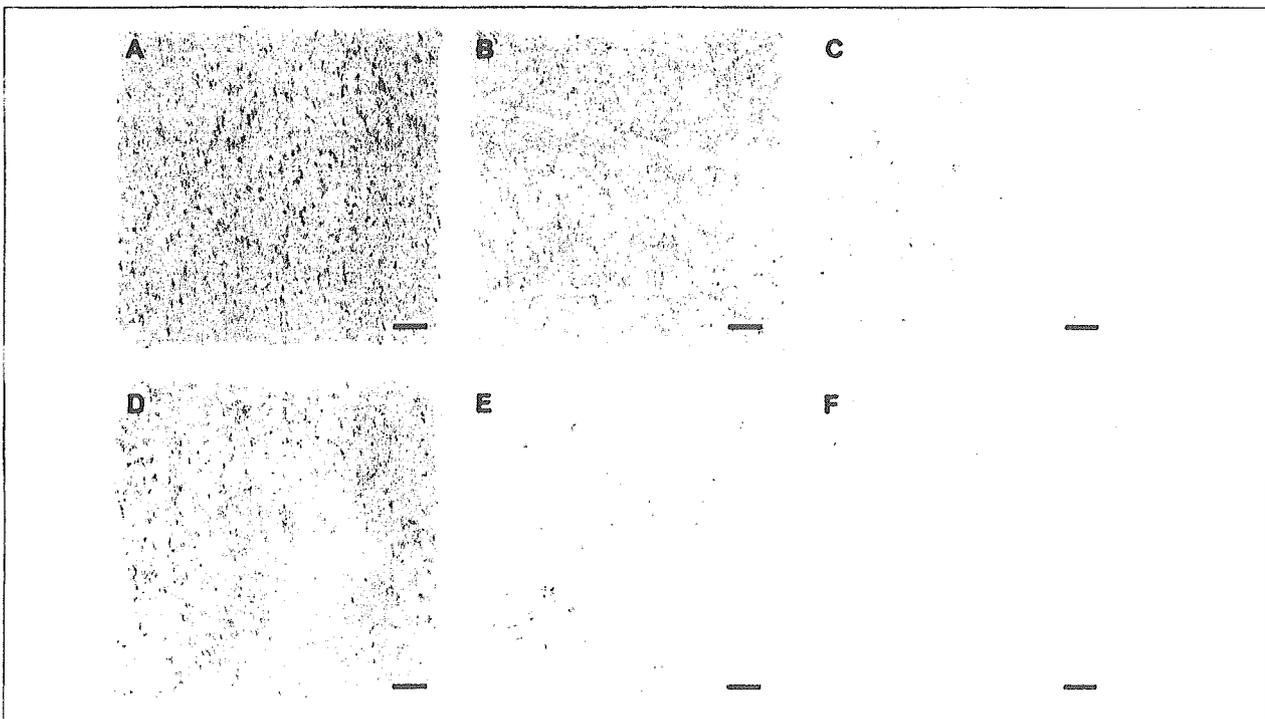

Figure 6. Histopathology of anterior tibial muscles. H&E staining of cross-sections of anterior tibial muscles from normal G3 male at 3 days of age (**A**), 2 month of age (**B**), and 6 months of age (**C**), and from affected G3 male at 3 days of age (**D**), 2 month of age (**E**), and 6 months of age (**F**). Bar = 50 μm
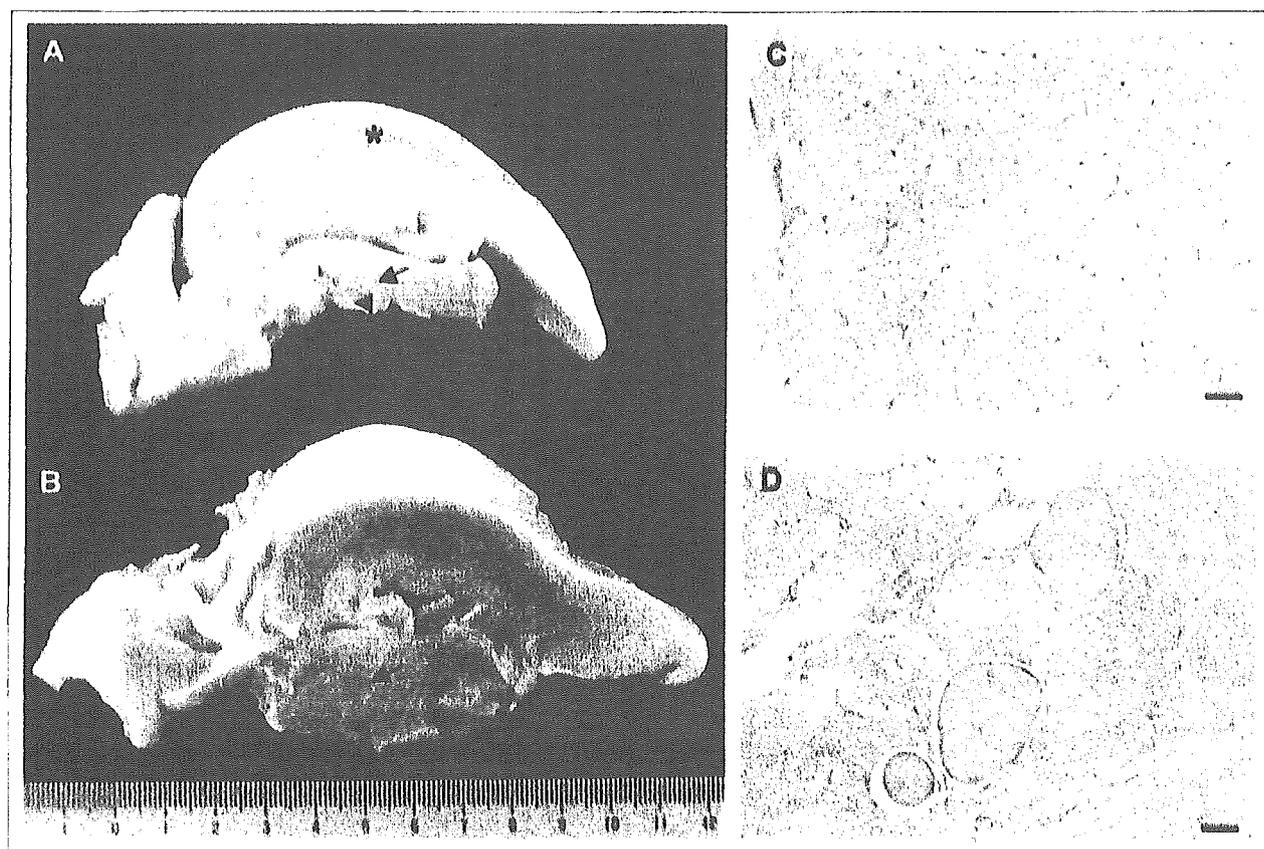
151

Figure 7. Macroscopy and histopathology of tongue and sublingual muscles. Tongue (asterisk), genioglossus (arrow) and geniohyoideus (arrowhead) muscles in a normal G3 male (A) and an affected G3 male (B) at 12 months of age. Bar = 1 cm. H&E staining of cross-sections of the tongue muscle from a normal G3 male (C) and an affected G3 male (D) at 12 months of age. Bar = 50 μm.

dealt mainly with the third generation of dystrophic dogs, G3, when they still have mixture of both beagle and golden retriever backgrounds. However, the size of G3 CXMD₁ was smaller and easier to handle than golden retriever-based CXMD dogs [16].

The serum CK levels in affected G3 dogs reached two peaks during the course: the first peak occurred immediately after birth and the second peak at two months after birth. This particular pattern of serum CK levels was also seen in G3 carrier females, although the increase was quite small. Previous researchers have reported that serum CK levels in CXMD dogs were much higher than those in normal littermates shortly after birth [15, 17] and had another peak at 6 to 8 weeks after birth [15]. The profiles of serum CK levels in our dystrophic G3 dogs corresponded well with these reports.

The elevation of serum CK levels in G3 affected and carrier female dogs shortly after birth

may be a result of acute generalized muscle damage after the stress of whelping. It is very important to note that 32.3% of affected G3 male pups had died by 3 days of age, and the rate was significantly higher than that of normal dogs. Actually, it has been reported that 28.0% or 45.5% CXMD pups died with a neonatal fulminant form within the first 2 weeks after birth [15, 18]. Although the cause has not been fully elucidated, acute respiratory failure might be associated with the pathogenesis of the early death because involvement of the diaphragm muscle was seen in neonatal fulminant CXMD pups [19] as well as in affected G3 dogs at three days after birth (Fig. 5E). The stress of whelping is one factor that may exacerbate involvement of the diaphragm. Moreover, Nguyen et al. reported selective involvement of the diaphragm muscle in neonatal CXMD pups, and they found that anterior tibial muscle damage was not more severe than that of the diaphragm muscle [19]. In affected G3 dogs, a similar selec-

152